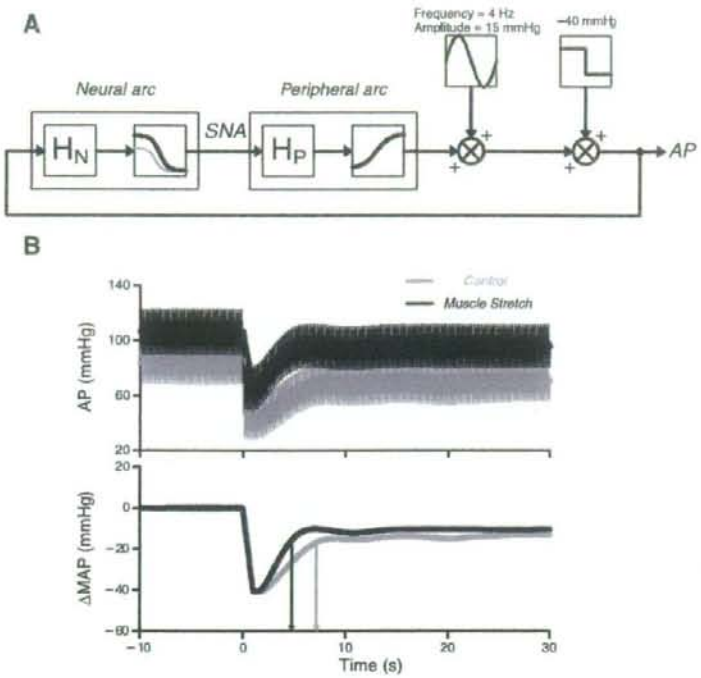

Fig. 6. *A*: simulator of the baroreflex system during activation of the muscle mechanoreflex. A stepwise perturbation with pulsatile pressure was applied to the baroreflex negative feedback system (see the APPENDIX for details). H_N, neural arc transfer function; H_P, peripheral arc transfer function. *B*: simulation results of the closed-loop AP response to the stepwise pressure perturbation (−40 mmHg). Muscle stretch shortened the time to 95% of steady state by −33% (shaded and solid arrows). Shaded and solid thick lines indicate mean AP (MAP) resampled at 1 Hz. ΔMAP, change in MAP from baseline.

steadily diminishing. In fact, the increase in SNA and AP induced by muscle stretch gradually decreased from 90 s to 6 min after the initiation of the muscle stretch, which was used for data analysis (Table 1). However, SNA and AP remained significantly higher under muscle stretch conditions than control conditions over the protocol for 6 min. Thus, we believe that the mechanoreflex remained activated in this protocol. Further studies are required to elucidate the dynamic interactions between baroreflex and mechanoreflex induced by different modes of activation, such as cyclic activation of the mechanoreflex.

Third, the transfer function analysis is useful in identifying the linear input-output relationship of the baroreflex at a given operating point. However, the transfer function cannot characterize the nonlinear input-output relationship of the system. In the presence of nonlinear system behavior such as the baroreflex system, the transfer function analysis is partly compromised, indicating that the absolute output values of the nonlinear system to given input signals cannot be predicted accurately by the transfer function alone. Combining a linear transfer function with a nonlinear sigmoidal element would increase the accuracy to reproduce dynamic characteristics observed in the baroreflex neural arc (20, 22).

Finally, we measured renal SNA as a proxy of systemic sympathetic activity. SNAs to different organs may vary a lot. Although static and dynamic regulations of the baroreflex neural arc are similar among renal, cardiac, and muscle SNAs (15, 16, 18), whether this holds true during muscle stretch remains to be verified. Also, subsystems of the peripheral arc transfer function such as those relating cardiac output and peripheral vascular resistance remain to be identified.

Conclusions. In conclusion, baroreflex open-loop transfer function analysis demonstrated that the activation of mechanosensitive afferents from skeletal muscles augmented the dynamic SNA response in the neural arc. This augmentation of the dynamic SNA response with maintained derivative characteristics of the neural arc may accelerate closed-loop AP regulation via the baroreflex.

APPENDIX

To simulate the closed-loop AP response to stepwise pressure perturbation (Fig. 6), we used the derivative-sigmoidal cascade model. The cascade model consists of a linear derivative filter followed by a nonlinear sigmoidal component (20, 22).

We modeled the sigmoidal nonlinearity in the baroreflex neural arc interacting with the muscle mechanoreflex by the following four-parameter logistic function with threshold according to a previous study (59):

$$y = \max\left\{\frac{P_1}{1+\exp[P_2(x-P_3)]} + P_4,\ \mathrm{Th}\right\} \qquad (A1)$$

where x and y are input (in mmHg) and output (in au) values. P_1 denotes the response range (in au), P_2 is the coefficient of gain, P_3 is the midpoint of the input range (in mmHg), P_4 is the minimum output value of the symmetric sigmoid curve (in au), and Th is a threshold value for the output (in au). The function $\max\{a,b\}$ gives the greater or equal value between a and b. We set $P_1 = 135$ au, $P_2 = 0.13$, $P_3 = 110$ mmHg, $P_4 = -40$ au, and Th = 0 au. Under muscle stretch conditions, the value of P_4 was changed to 5 au. These settings were determined based on the static interaction

between the baroreflex and muscle mechanoreflex obtained from previous studies (58, 59).

The sigmoidal nonlinearity in the peripheral arc was modelled by a four-parameter logistic function as follows:

$$z = \frac{Q_1}{1 + \exp[Q_2(y - Q_3)]} + Q_4 \qquad (A2)$$

where y and z are input (in au) and output (in mmHg) values. Q_1 denotes the response range (in mmHg), Q_2 is the coefficient of gain, Q_3 is the midpoint of the input range (in au), and Q_4 is the minimum output value (in mmHg). We set $Q_1 = 120$ mmHg, $Q_2 = -0.05$, $Q_3 = 70$ au, and $Q_4 = 30$ mmHg under both conditions, according to a previous study (58).

The neural arc (H_N) and peripheral arc (H_P) linear transfer functions under control and muscle stretch conditions were obtained from Fig. 2. Because absolute values of the steady-state gains in the neural and peripheral arcs were determined by a sigmoid curve (*Eqs. A1* and *A2*), the steady-state gains of H_N and H_P under both conditions were normalized to unity.

The input amplitude of the stepwise pressure perturbation was −40 mmHg. To mimic pulsatile pressure, we imposed a sinusoidal input on the output from the peripheral arc. The frequency and zero to peak amplitude of the sinusoidal input were 4 Hz and 15 mmHg, respectively (Fig. 6*A*). The closed-loop AP response was simulated up to 30 s (Fig. 6*B*).

GRANTS

This work was supported by Ministry of Health, Labour and Welfare of Japan Health and Labour Sciences Research Grant for Research on Advanced Medical Technology, Health and Labour Sciences Research Grant for Research on Medical Devices for Analyzing, Supporting and Substituting the Function of Human Body, and Health and Labour Sciences Research Grants H18-Iryo-Ippan-023 and H18-Nano-Ippan-003; the Industrial Technology Research Grant Program of the New Energy and Industrial Technology Development Organization of Japan; and Ministry of Education, Culture, Sports, Science and Technology Grant-In-Aid for Scientific Research 18591992.

REFERENCES

1. **Charkoudian N, Martin EA, Dinenno FA, Eisenach JH, Dietz NM, Joyner MJ.** Influence of increased central venous pressure on baroreflex control of sympathetic activity in humans. *Am J Physiol Heart Circ Physiol* 287: H1658–H1662, 2004.
2. **Chen CY, Horowitz JM, Bonham AC.** A presynaptic mechanism contributes to depression of autonomic signal transmission in NTS. *Am J Physiol Heart Circ Physiol* 277: H1350–H1360, 1999.
3. **Fadel PJ, Ogoh S, Watenpaugh DE, Wasmund W, Olivencia-Yurvati A, Smith ML, Raven PB.** Carotid baroreflex regulation of sympathetic nerve activity during dynamic exercise in humans. *Am J Physiol Heart Circ Physiol* 280: H1383–H1390, 2001.
4. **Gallagher KM, Fadel PJ, Smith SA, Norton KH, Querry RG, Olivencia-Yurvati A, Raven PB.** Increases in intramuscular pressure raise arterial blood pressure during dynamic exercise. *J Appl Physiol* 91: 2351–2358, 2001.
5. **Gallagher KM, Fadel PJ, Stromstad M, Ide K, Smith SA, Querry RG, Raven PB, Secher NH.** Effects of exercise pressor reflex activation on carotid baroreflex function during exercise in humans. *J Physiol* 533: 871–880, 2001.
6. **Gallagher KM, Fadel PJ, Stromstad M, Ide K, Smith SA, Querry RG, Raven PB, Secher NH.** Effects of partial neuromuscular blockade on carotid baroreflex function during exercise in humans. *J Physiol* 533: 861–870, 2001.
7. **Hayes SG, Kaufman MP.** Gadolinium attenuates exercise pressor reflex in cats. *Am J Physiol Heart Circ Physiol* 280: H2153–H2161, 2001.
8. **Hayes SG, Kindig AE, Kaufman MP.** Comparison between the effect of static contraction and tendon stretch on the discharge of group III and IV muscle afferents. *J Appl Physiol* 99: 1891–1896, 2005.
9. **Ichinose M, Saito M, Fujii N, Ogawa T, Hayashi K, Kondo N, Nishiyasu T.** Modulation of the control of muscle sympathetic nerve activity during incremental leg cycling. *J Physiol* 586: 2753–2766, 2008.
10. **Ichinose M, Saito M, Kondo N, Nishiyasu T.** Time-dependent modulation of arterial baroreflex control of muscle sympathetic nerve activity during isometric exercise in humans. *Am J Physiol Heart Circ Physiol* 290: H1419–H1426, 2006.
11. **Ichinose M, Saito M, Wada H, Kitano A, Kondo N, Nishiyasu T.** Modulation of arterial baroreflex control of muscle sympathetic nerve activity by muscle metaboreflex in humans. *Am J Physiol Heart Circ Physiol* 286: H701–H707, 2004.
12. **Ichinose M, Saito M, Wada H, Kitano A, Kondo N, Nishiyasu T.** Modulation of arterial baroreflex dynamic response during muscle metaboreflex activation in humans. *J Physiol* 544: 939–948, 2002.
13. **Iellamo F, Legramante JM, Raimondi G, Peruzzi G.** Baroreflex control of sinus node during dynamic exercise in humans: effects of central command and muscle reflexes. *Am J Physiol Heart Circ Physiol* 272: H1157–H1164, 1997.
14. **Ikeda Y, Kawada T, Sugimachi M, Kawaguchi O, Shishido T, Sato T, Miyano H, Matsuura W, Alexander J Jr, Sunagawa K.** Neural arc of baroreflex optimizes dynamic pressure regulation in achieving both stability and quickness. *Am J Physiol Heart Circ Physiol* 271: H882–H890, 1996.
15. **Kamiya A, Kawada T, Yamamoto K, Michikami D, Ariumi H, Miyamoto T, Shimizu S, Uemura K, Aiba T, Sunagawa K, Sugimachi M.** Dynamic and static baroreflex control of muscle sympathetic nerve activity (SNA) parallels that of renal and cardiac SNA during physiological change in pressure. *Am J Physiol Heart Circ Physiol* 289: H2641–H2648, 2005.
16. **Kamiya A, Kawada T, Yamamoto K, Michikami D, Ariumi H, Miyamoto T, Uemura K, Sugimachi M, Sunagawa K.** Muscle sympathetic nerve activity averaged over 1 minute parallels renal and cardiac sympathetic nerve activity in response to a forced baroreceptor pressure change. *Circulation* 112: 384–386, 2005.
17. **Kamiya A, Michikami D, Fu Q, Niimi Y, Iwase S, Mano T, Suzumura A.** Static handgrip exercise modifies arterial baroreflex control of vascular sympathetic outflow in humans. *Am J Physiol Regul Integr Comp Physiol* 281: R1134–R1139, 2001.
18. **Kawada T, Shishido T, Inagaki M, Tatewaki T, Zheng C, Yanagiya Y, Sugimachi M, Sunagawa K.** Differential dynamic baroreflex regulation of cardiac and renal sympathetic nerve activities. *Am J Physiol Heart Circ Physiol* 280: H1581–H1590, 2001.
19. **Kawada T, Shishido T, Inagaki M, Zheng C, Yanagiya Y, Uemura K, Sugimachi M, Sunagawa K.** Estimation of baroreflex gain using a baroreflex equilibrium diagram. *Jpn J Physiol* 52: 21–29, 2002.
20. **Kawada T, Uemura K, Kashihara K, Kamiya A, Sugimachi M, Sunagawa K.** A derivative-sigmoidal model reproduces operating point-dependent baroreflex neural arc transfer characteristics. *Am J Physiol Heart Circ Physiol* 286: H2272–H2279, 2004.
21. **Kawada T, Yamamoto K, Kamiya A, Ariumi H, Michikami D, Shishido T, Sunagawa K, Sugimachi M.** Dynamic characteristics of carotid sinus pressure-nerve activity transduction in rabbits. *Jpn J Physiol* 55: 157–163, 2005.
22. **Kawada T, Yanagiya Y, Uemura K, Miyamoto T, Zheng C, Li M, Sugimachi M, Sunagawa K.** Input-size dependence of the baroreflex neural arc transfer characteristics. *Am J Physiol Heart Circ Physiol* 284: H404–H415, 2003.
23. **Kawada T, Zheng C, Yanagiya Y, Uemura K, Miyamoto T, Inagaki M, Shishido T, Sugimachi M, Sunagawa K.** High-cut characteristics of the baroreflex neural arc preserve baroreflex gain against pulsatile pressure. *Am J Physiol Heart Circ Physiol* 282: H1149–H1156, 2002.
24. **Keller DM, Fadel PJ, Ogoh S, Brothers RM, Hawkins M, Olivencia-Yurvati A, Raven PB.** Carotid baroreflex control of leg vasculature in exercising and non-exercising skeletal muscle in humans. *J Physiol* 561: 283–293, 2004.
25. **Leshnower BG, Potts JT, Garry MG, Mitchell JH.** Reflex cardiovascular responses evoked by selective activation of skeletal muscle ergoreceptors. *J Appl Physiol* 90: 308–316, 2001.
26. **Liu Z, Chen CY, Bonham AC.** Frequency limits on aortic baroreceptor input to nucleus tractus solitarii. *Am J Physiol Heart Circ Physiol* 278: H577–H585, 2000.
27. **Marmarelis PZ, Marmarelis VZ.** The white noise method in system identification. In: *Analysis of Physiological Systems*. New York: Plenum, 1978, p. 131–221.
28. **Matsukawa K, Nakamoto T, Inomoto A.** Gadolinium does not blunt the cardiovascular responses at the onset of voluntary static exercise in cats: a predominant role of central command. *Am J Physiol Heart Circ Physiol* 292: H121–H129, 2007.

29. **McIlveen SA, Hayes SG, Kaufman MP.** Both central command and exercise pressor reflex reset carotid sinus baroreflex. *Am J Physiol Heart Circ Physiol* 280: H1454–H1463, 2001.
30. **Melcher A, Donald DE.** Maintained ability of carotid baroreflex to regulate arterial pressure during exercise. *Am J Physiol Heart Circ Physiol* 241: H838–H849, 1981.
31. **Mense S, Stahnke M.** Responses in muscle afferent fibres of slow conduction velocity to contractions and ischaemia in the cat. *J Physiol* 342: 383–397, 1983.
32. **Miki K, Yoshimoto M, Tanimizu M.** Acute shifts of baroreflex control of renal sympathetic nerve activity induced by treadmill exercise in rats. *J Physiol* 548: 313–322, 2003.
33. **Miles R.** Frequency dependence of synaptic transmission in nucleus of the solitary tract in vitro. *J Neurophysiol* 55: 1076–1090, 1986.
34. **Mohrman DE, Heller LJ.** Regulation of arterial pressure. In: *Cardiovascular Physiology* (4th ed.). New York: McGraw-Hill, 1997, p. 158–230.
35. **Norton KH, Boushel R, Strange S, Saltin B, Raven PB.** Resetting of the carotid arterial baroreflex during dynamic exercise in humans. *J Appl Physiol* 87: 332–338, 1999.
36. **Ogoh S, Fisher JP, Dawson EA, White MJ, Secher NH, Raven PB.** Autonomic nervous system influence on arterial baroreflex control of heart rate during exercise in humans. *J Physiol* 566: 599–611, 2005.
37. **Ogoh S, Fisher JP, Fadel PJ, Raven PB.** Increases in central blood volume modulate carotid baroreflex resetting during dynamic exercise in humans. *J Physiol* 581: 405–418, 2007.
38. **Ogoh S, Fisher JP, Raven PB, Fadel PJ.** Arterial baroreflex control of muscle sympathetic nerve activity in the transition from rest to steady-state dynamic exercise in humans. *Am J Physiol Heart Circ Physiol* 293: H2202–H2209, 2007.
39. **Ogoh S, Wasmund WL, Keller DM, AOY, Gallagher KM, Mitchell JH, Raven PB.** Role of central command in carotid baroreflex resetting in humans during static exercise. *J Physiol* 543: 349–364, 2002.
40. **Papelier Y, Escourrou P, Gauthier JP, Rowell LB.** Carotid baroreflex control of blood pressure and heart rate in men during dynamic exercise. *J Appl Physiol* 77: 502–506, 1994.
41. **Papelier Y, Escourrou P, Helloco F, Rowell LB.** Muscle chemoreflex alters carotid sinus baroreflex response in humans. *J Appl Physiol* 82: 577–583, 1997.
42. **Potts JT, Hand GA, Li J, Mitchell JH.** Central interaction between carotid baroreceptors and skeletal muscle receptors inhibits sympathoexcitation. *J Appl Physiol* 84: 1158–1165, 1998.
43. **Potts JT, Li J.** Interaction between carotid baroreflex and exercise pressor reflex depends on baroreceptor afferent input. *Am J Physiol Heart Circ Physiol* 274: H1841–H1847, 1998.
44. **Potts JT, Mitchell JH.** Rapid resetting of carotid baroreceptor reflex by afferent input from skeletal muscle receptors. *Am J Physiol Heart Circ Physiol* 275: H2000–H2008, 1998.
45. **Potts JT, Shi XR, Raven PB.** Carotid baroreflex responsiveness during dynamic exercise in humans. *Am J Physiol Heart Circ Physiol* 265: H1928–H1938, 1993.
46. **Querry RG, Smith SA, Stromstad M, Ide K, Raven PB, Secher NH.** Neural blockade during exercise augments central command's contribution to carotid baroreflex resetting. *Am J Physiol Heart Circ Physiol* 280: H1635–H1644, 2001.
47. **Rowell LB, O'Leary DS.** Reflex control of the circulation during exercise: chemoreflexes and mechanoreflexes. *J Appl Physiol* 69: 407–418, 1990.
48. **Sato T, Kawada T, Inagaki M, Shishido T, Takaki H, Sugimachi M, Sunagawa K.** New analytic framework for understanding sympathetic baroreflex control of arterial pressure. *Am J Physiol Heart Circ Physiol* 276: H2251–H2261, 1999.
49. **Smith SA, Querry RG, Fadel PJ, Gallagher KM, Stromstad M, Ide K, Raven PB, Secher NH.** Partial blockade of skeletal muscle somatosensory afferents attenuates baroreflex resetting during exercise in humans. *J Physiol* 551: 1013–1021, 2003.
50. **Stebbins CL, Brown B, Levin D, Longhurst JC.** Reflex effect of skeletal muscle mechanoreceptor stimulation on the cardiovascular system. *J Appl Physiol* 65: 1539–1547, 1988.
51. **Sugimachi M, Imaizumi T, Sunagawa K, Hirooka Y, Todaka K, Takeshita A, Nakamura M.** A new method to identify dynamic transduction properties of aortic baroreceptors. *Am J Physiol Heart Circ Physiol* 258: H887–H895, 1990.
52. **Suzuki S, Ando S, Imaizumi T, Takeshita A.** Effects of anesthesia on sympathetic nerve rhythm: power spectral analysis. *J Auton Nerv Syst* 43: 51–58, 1993.
53. **Terui N, Masuda N, Saeki Y, Kumada M.** Activity of barosensitive neurons in the caudal ventrolateral medulla that send axonal projections to the rostral ventrolateral medulla in rabbits. *Neurosci Lett* 118: 211–214, 1990.
54. **Vatner SF, Braunwald E.** Cardiovascular control mechanisms in the conscious state. *N Engl J Med* 293: 970–976, 1975.
55. **Vatner SF, Franklin D, Braunwald E.** Effects of anesthesia and sleep on circulatory response to carotid sinus nerve stimulation. *Am J Physiol* 220: 1249–1255, 1971.
56. **Vatner SF, Franklin D, Van Citters RL, Braunwald E.** Effects of carotid sinus nerve stimulation on blood-flow distribution in conscious dogs at rest and during exercise. *Circ Res* 27: 495–503, 1970.
57. **Wray DW, Fadel PJ, Keller DM, Ogoh S, Sander M, Raven PB, Smith ML.** Dynamic carotid baroreflex control of the peripheral circulation during exercise in humans. *J Physiol* 559: 675–684, 2004.
58. **Yamamoto K, Kawada T, Kamiya A, Takaki H, Miyamoto T, Sugimachi M, Sunagawa K.** Muscle mechanoreflex induces the pressor response by resetting the arterial baroreflex neural arc. *Am J Physiol Heart Circ Physiol* 286: H1382–H1388, 2004.
59. **Yamamoto K, Kawada T, Kamiya A, Takaki H, Sugimachi M, Sunagawa K.** Static interaction between muscle mechanoreflex and arterial baroreflex in determining efferent sympathetic nerve activity. *Am J Physiol Heart Circ Physiol* 289: H1604–H1609, 2005.

REGULAR PAPER

J. Physiol. Sci. Vol. 58, No. 3; Jun. 2008; pp. 189–198
Online May 13, 2008; **doi:10.2170/physiolsci.RP004308**

Upright Tilt Resets Dynamic Transfer Function of Baroreflex Neural Arc to Minify the Pressure Disturbance in Total Baroreflex Control

Atsunori KAMIYA[1], Toru KAWADA[1], Kenta YAMAMOTO[2], Masaki MIZUNO[1], Shuji SHIMIZU[1], and Masaru SUGIMACHI[1]

[1]Department of Cardiovascular Dynamics, National Cardiovascular Centre Research Institute, Osaka, Japan; and [2]Consolidated Research Institute for Advanced Science and Medical Care, Waseda University, Tokyo ,162-0041 Japan

Reprinted from
The Journal of Physiological Sciences
Volume 58, Number 3, pp. 189–198, 2008
http://jps.physiology.jp/ doi:10.2170/physiolsci.RP004308

Published by The Physiological Society of Japan

Received on Mar 18, 2008; accepted on May 9, 2008; released online on May 13, 2008; doi:10.2170/physiolsci.RP004308
Correspondence should be addressed to: Atsunori Kamiya, Department of Cardiovascular Dynamics, National Cardiovascular Centre Research Institute, Osaka, 565-8565 Japan. Tel: +81-6-6833-5012, Fax: +81-6-6835-5403, E-mail: kamiya@ri.ncvc.go.jp

REGULAR PAPER

J. Physiol. Sci. Vol. 58, No. 3; Jun. 2008; pp. 189–198
Online May 13, 2008; doi:10.2170/physiolsci.RP004308

Upright Tilt Resets Dynamic Transfer Function of Baroreflex Neural Arc to Minify the Pressure Disturbance in Total Baroreflex Control

Atsunori KAMIYA[1], Toru KAWADA[1], Kenta YAMAMOTO[2], Masaki MIZUNO[1], Shuji SHIMIZU[1], and Masaru SUGIMACHI[1]

[1]Department of Cardiovascular Dynamics, National Cardiovascular Centre Research Institute, Osaka, Japan; and [2]Consolidated Research Institute for Advanced Science and Medical Care, Waseda University, Tokyo ,162-0041 Japan

Abstract: Maintenance of arterial pressure (AP) under orthostatic stress against gravitational fluid shift and pressure disturbance is of great importance. One of the mechanisms is that upright tilt resets steady-state baroreflex control to a higher sympathetic nerve activity (SNA). However, the dynamic feedback characteristics of the baroreflex system, a hallmark of fast-acting neural control, remain to be elucidated. In the present study, we tested the hypothesis that upright tilt resets the dynamic transfer function of the baroreflex neural arc to minify the pressure disturbance in total baroreflex control. Renal SNA and AP were recorded in ten anesthetized, vagotomized and aortic-denervated rabbits. Under baroreflex open-loop condition, isolated intracarotid sinus pressure (CSP) was changed according to a binary white noise sequence at operating pressure ± 20 mmHg, while the animal was placed supine and at 60° upright tilt. Regardless of the postures, the baroreflex neural (CSP to SNA) and peripheral (SNA to AP) arcs showed dynamic high-pass and low-pass characteristics, respectively. Upright tilt increased the transfer gain of the neural arc (resetting), decreased that of the peripheral arc, and consequently maintained the transfer characteristics of total baroreflex feedback system. A simulation study suggests that postural resetting of the neural arc would significantly increase the transfer gain of the total arc in upright position, and that in closed-loop baroreflex the resetting increases the stability of AP against pressure disturbance under orthostatic stress. In conclusion, upright tilt resets the dynamic transfer function of the baroreflex neural arc to minify the pressure disturbance in total baroreflex control.

Key words: baroreflex, blood pressure, sympathetic nervous system.

Since human beings are often under orthostatic stress, the maintenance of arterial pressure (AP) under orthostatic stress against gravitational fluid shift is of great importance. During standing, a gravitational fluid shift directed toward the lower part of the body would cause severe postural hypotension if not counteracted by compensatory mechanisms [1]. Arterial baroreflex has been considered to be the major compensatory mechanism [1–3], since denervation of baroreceptor afferents causes profound postural hypotension [4].

The baroreflex system consists of two subsystems: the neural arc that represents the input-output relationship between baroreceptor pressure and sympathetic nerve activity (SNA), and the peripheral arc that represents the relationship between SNA and systemic AP. Recently, we investigated the steady-state functional structure of these systems under orthostatic stress [5], and reported that upright tilt shifted the baroreflex peripheral arc to a lower AP for a given SNA. However, upright tilt reset the baroreflex neural arc to a higher steady state SNA. The resetting compensated for the blunted responsiveness of the peripheral arc and contributed to prevent postural hypotension [5].

In addition to the steady state characteristics [6, 7], the dynamic characteristics are other hallmark of the baroreflex system. It is because the system is a fast-acting neural control that quickly negative-feedback controls and stabilises AP against pressure disturbance in contrast to the slow-acting hormonal and humoral systems [8]. Earlier studies reported that the dynamic characteristics in supine position have a high-pass (fast) neural arc that may compensate for the low-pass (slow) peripheral arc to achieve rapid and stable AP regulation [8]. The importance of the dynamic characteristics in AP control increases under orthostatic stress that can cause postural hypotension. However, little is known about the dynamic characteristics of the baroreflex system in upright posture.

Because the gravitational body fluid shift decreases the effective circulatory blood volume [1, 9], we speculated that upright tilt may attenuate the dynamic transfer function from SNA to AP in the baroreflex peripheral arc.

Received on Mar 18, 2008; accepted on May 9, 2008; released online on May 13, 2008; doi:10.2170/physiolsci.RP004308
Correspondence should be addressed to: Atsunori Kamiya, Department of Cardiovascular Dynamics, National Cardiovascular Centre Research Institute, Osaka, 565-8565 Japan. Tel: +81-6-6833-5012, Fax: +81-6-6835-5403, E-mail: kamiya@ri.ncvc.go.jp

Moreover, if the upright tilt resets the dynamic characteristics of the neural arc in addition to resetting the steady state SNA reported previously [5], it would compensate for a blunted pressor response of the baroreflex peripheral arc and contribute to maintain the stability and quickness of the total baroreflex system. Accordingly, we hypothesized that upright tilt resets dynamic transfer function of baroreflex neural arc to minify the pressure disturbance in total baroreflex control.

In the present study, we identified the transfer functions of two baroreflex subsystems (the neural and peripheral arcs) separately in 60° upright posture, while opening the baroreflex negative feedback loop by vascular isolation of carotid sinus regions [8]. In addition, by connecting the subsystem transfer functions in series and closing them, we investigated the dynamic transfer characteristics and the stability against pressure disturbance of total baroreflex arc system in upright posture.

MATERIAL AND METHODS

Animals were cared for in strict accordance with the Guiding Principles for the Care and Use of Animals in the Field of Physiological Science approved by the Physiological Society of Japan. Ten Japanese white rabbits weighing 2.4–3.3 kg were initially anesthetized by intravenous injection (2 ml/kg) of a mixture of urethane (250 mg/ml) and α-chloralose (40 mg/ml). Anesthesia was maintained by continuously infusing the anaesthetics at a rate of 0.33 ml/kg/h using a syringe pump (CFV-3200, Nihon Kohden, Tokyo). The rabbits were mechanically ventilated with oxygen-enriched room air. Bilateral carotid sinuses were isolated vascularly from systemic circulation by ligating the internal and external carotid arteries and other small branches originating from the carotid sinus regions. The isolated carotid sinuses were filled with warmed physiological saline pre-equilibrated with atmospheric air, through catheters inserted via the common carotid arteries. Intra-carotid sinus pressure (CSP) was controlled by a servo-controlled piston pump (model ET-126A, Labworks; Costa Mesa, CA). Bilateral vagal and aortic depressor nerves were sectioned in the middle of the neck region to eliminate reflexes from the cardiopulmonary region and the aortic arch. Systemic AP was measured using a high-fidelity pressure transducer (Millar Instruments; Houston, TX) inserted retrograde from the right common carotid artery below the isolated carotid sinus region. Body temperature was maintained at around 38°C with a heating pad.

The left renal sympathetic nerve was exposed retroperitoneally. A pair of stainless steel wire electrodes (Bioflex wire AS633, Cooner Wire) was attached to the nerve to record renal SNA. The nerve fibers peripheral to electrodes were ligated securely and crushed to eliminate afferent signals. The nerve and electrodes were covered with a mixture of silicone gel (Silicon Low Viscosity, KWIK-SIL, World Precision Instrument, Inc., FL) to insulate and immobilize the electrodes. The preamplified SNA signal was band-pass filtered at 150–1,000 Hz. The nerve signal was full-wave rectified and low-pass filtered with a cutoff frequency of 30 Hz to quantify the nerve activity.

Protocols. Both protocols 1 and 2 were performed on each of eight animals. After the surgical preparation, the animal was maintained supine (0°) on a tilt bed. To stabilize the posture, the head was fixed full-frontal to the bed by strings, and the body and legs were rigged up in a clothes-like bag. Before performing protocols 1 and 2, we confirmed that the nerve activity measured in supine position was SNA. CSP was decreased stepwise from 100 mmHg to 40 mmHg in decrements of 20 mmHg, and then increased stepwise to 100 mmHg in increments of 20 mmHg. Each pressure step was maintained for 60 s. In all animals, a decrease in CSP increased SNA, whereas an increase in CSP decreased SNA (Fig. 1), indicating that the nerve activity recorded was SNA.

Protocol 1: The animal was placed supine. CSP was firstly matched with systemic AP to obtain the operating AP under the baroreflex closed-loop condition. After at least 5 minutes of stabilization, the SNA and AP were recorded for 10 min to obtain closed-loop baseline values. The data were stored on the hard disk of a dedicated laboratory computer system for analysis at a sampling rate of 200 Hz using a 12-bit analog-to-digital converter. The averaged AP over 10 min was defined as the operating AP in

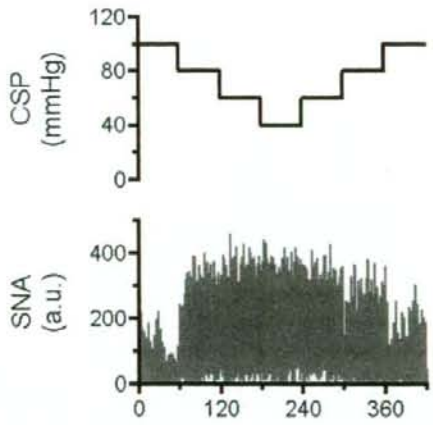

Fig. 1. Representative data of one rabbit in supine position, showing time series of carotid sinus pressure (CSP) and sympathetic nerve activity (SNA). CSP was decreased stepwise from 100 mmHg to 40 mmHg in decrements of 20 mmHg, and then increased stepwise to 100 mmHg in increments of 20 mmHg. Each pressure step was maintained for 60 s. A decrease in CSP increased SNA, whereas an increase in CSP decreased SNA, indicating that the nerve activity recorded was SNA. a.u., arbitrary unit.

supine position. Then, after at least 5 min of stabilization, CSP was randomly changed by 20 mmHg above or below the operating AP every 500 ms according to a binary white noise sequence for which the input power spectrum of CSP was reasonably flat up to 1 Hz [10]. The variables were recorded for a 10-min period and stored.

Protocol 2: CSP was firstly matched with systemic AP via a servo-controlled piston pump to obtain the actual operating pressure under baroreflex closed-loop conditions in supine and 60° upright postures. The animal was maintained supine for 10 min, and then tilted upright to 60° within 10 s by inclining the tilt bed to 60° and dropping the lower regions of the rabbit with the fulcrum set at the level of the carotid sinus. The 60° upright posture was maintained for 10 min for stabilization. Since the clothes-like bag stabilized the posture of the animal, there was no additional mechanical movement that reduced the quality of measurements. The position of the head remained almost fixed during the tilt to minimize vestibular stimulation. Thereafter, the average AP over the next 10 min was defined as the operating AP in upright tilt position. Then, after at least 5 min of stabilization, CSP was randomly changed according to a white noise sequence for 10 min as in protocol 1.

Data analysis. SNA signals were normalized by the following steps. First, the post-mortem noise level was assigned 0 arbitrary unit (a.u.). Second, SNA signals during the 10-min closed-loop baseline recording in protocol 1 (supine position) were averaged over 1 min, and assigned 100 a.u. Finally, the other SNA signals in all protocols were normalized to these values.

In both protocols 1 and 2, the transfer functions (gain and phase) and coherence function were calculated from CSP input to SNA in the baroreflex neural arc and from SNA input to AP in the baroreflex peripheral arc. The signals of CSP, SNA and AP were resampled at 10 Hz and segmented into 10 sets of 50% overlapping bins of 2^{10} data point each. The segment length was 102.4 s, which yielded the lowest frequency bound of 0.01 (0.0097) Hz. We subtracted a linear trend and applied a Hanning window for each segment. We then performed fast Fourier transform to obtain frequency spectra of the variables. We ensemble averaged the input power [$Sxx(f)$], output power [$Syy(f)$], and cross power between them [$Syx(f)$] over the 10 segments. Thereafter, we calculated the transfer function [$H(f)$] from input to output signals as follows,

$$H(f) = \frac{Syx(f)}{Sxx(f)}$$

To quantify the linear dependence between input to output signals in the frequency domain, we calculated the magnitude-squared coherence function [$Coh(f)$] as follows:

$$Coh(f) = \frac{|Syx(f)|^2}{Sxx(f)Syy(f)}$$

The coherence value ranges from zero to unity. Unity coherence indicates a perfect linear dependence between input and output signals, whereas zero coherence indicates total independence of these two signals.

Statistic analysis. All data are presented as means ± SD. Effects of upright tilt on baroreflex parameters were evaluated by repeated-measures analysis of variance. When the main effect was found to be significant, post hoc multiple comparisons were done using the Scheff's F-test to compare baroreflex controls between the supine and upright postures [11]. Differences were considered significant when $P < 0.05$.

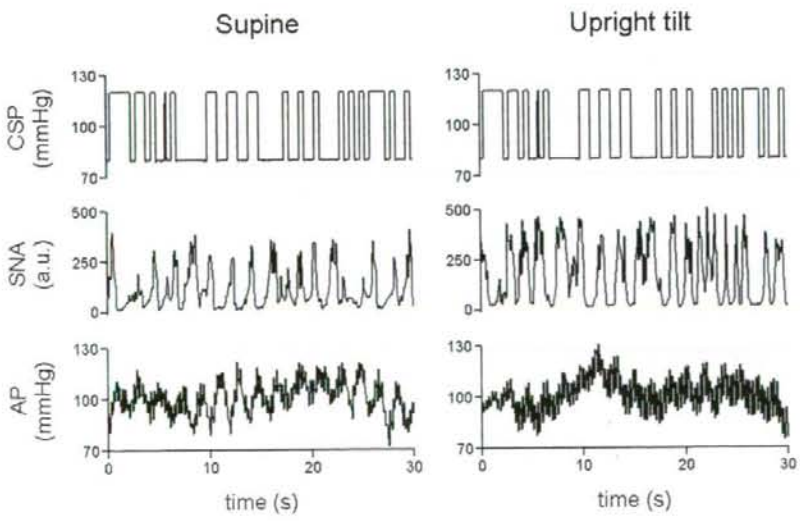

Fig. 2. Representative data of one rabbit in supine (left panels) and 60° upright tilt (right panels) positions, showing time series of carotid sinus pressure (CSP), sympathetic nerve activity (SNA) and systemic arterial pressure (AP) during CSP perturbation. CSP was changed according to a binary white noise signal with a switching interval of 500 ms. a.u., arbitrary unit.

RESULTS

Figure 2 shows the typical time series of CSP, SNA and AP derived in supine and 60° upright tilt positions in individual animal. CSP was perturbed according to a binary white noise sequence at 500-ms intervals. In both positions, SNA increased and decreased roughly in response to the decrease and increase in CSP, respectively. However, the SNA responses appeared higher in the upright tilt than in the supine position. Data from all animals ($n = 8$) showed that the upright tilt increased the averaged SNA (175 ± 21 a.u.) during CSP perturbation compared with the supine position (96 ± 13 a.u.). Averaged AP during CSP perturbation was similar in supine (96 ± 13 mmHg) and in upright positions (103 ± 15 mmHg).

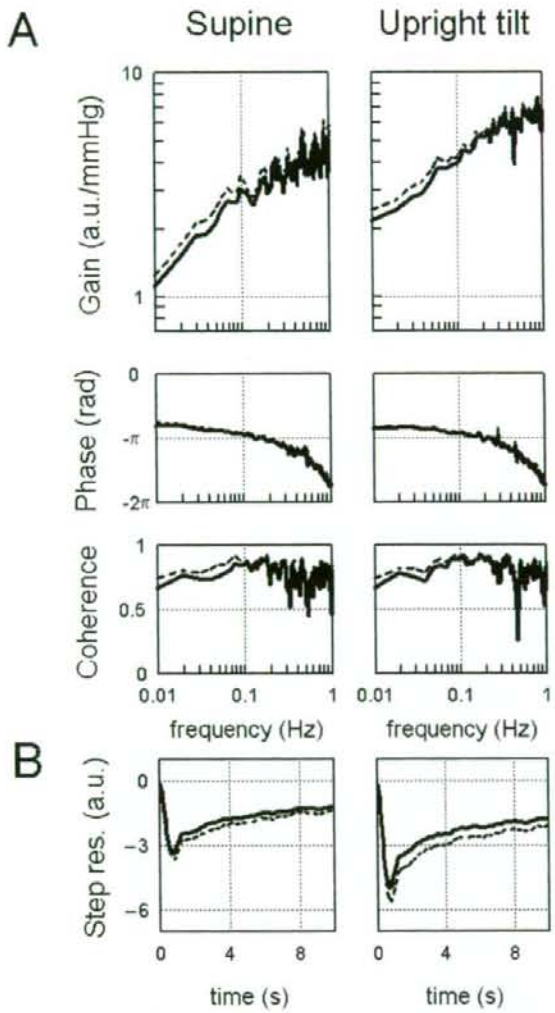

Fig. 3. A: The transfer function of the baroreflex neural arc from CSP to SNA averaged from all animals ($n = 8$) in supine (left panels) and 60° upright tilt (right panels) positions. The gain plots (top), phase plots (middle), and coherence function (bottom) are shown. Upright tilt increases the gain. **B**: Step responses (Step res.) derived from the transfer function corresponding to the transfer function shown in A. Upright tilt enhances the initial and steady-state responses. Solid line represents the mean values, and dashed line represents mean + SD in A and mean – SD in B. a.u., arbitrary unit.

The baroreflex neural arc

Figure 3A shows the transfer function of baroreflex neural arc from CSP to SNA averaged from all animals. In both supine and upright tilt positions, the transfer gain increased as the frequency of CSP perturbation increased for the frequency range of 0.01 to 1 Hz. This shows dynamic high-pass characteristics, indicating that more rapid change of CSP results in greater response of SNA. Note that upright tilt increased the transfer gain for the whole frequency range observed (Table 1). In addition, upright tilt decreased the slope of gain increase. In both positions, the phase approached slightly above $-\pi$ radians at the lowest frequency reflecting negative feedback characters, and lagged as the frequency of CSP perturbation increased. The coherence was over 0.7 for the frequency range of 0.01 to 0.2 Hz. Upright tilt did not affect the phase or coherence. Figure 3B shows the step response of SNA corresponding to the transfer function shown in Fig. 3A. In both positions, the SNA response consisted of an initial decrease followed by partial recovery and then a steady state. Of note, upright tilt enhanced the initial decrease by 50%, and also decreased the steady-state SNA.

Table 1. Transfer function of baroreflex neural arc (from CSP to SNA) in supine and upright tilt positions.

	Supine	Upright tilt
Gain (a.u./mmHg)		
0.01 Hz	1.11 ± 0.13	2.14 ± 0.41*
0.1 Hz	2.75 ± 0.43	4.63 ± 0.52*
0.3 Hz	3.69 ± 0.30	5.08 ± 0.42*
Phase (rad)		
0.01 Hz	–2.51 ± 0.15	–2.66 ± 0.09
0.1 Hz	–2.96 ± 0.08	–2.93 ± 0.06
0.3 Hz	–3.58 ± 0.14	–3.53 ± 0.12
Coherence		
0.01 Hz	0.67 ± 0.08	0.67 ± 0.07
0.1 Hz	0.84 ± 0.04	0.89 ± 0.02
0.3 Hz	0.77 ± 0.06	0.82 ± 0.03
Slope (dB/decade)		
0.01 Hz to 0.3 Hz	7.0 ± 0.4	5.1 ± 0.5*
Step response (a.u.)		
Initial response	–3.41 ± 0.21	–4.99 ± 0.62*
Steady-state level	–1.26 ± 0.18	–1.80 ± 0.32*

Values are mean ± SD ($n = 10$). *$P < 0.05$; supine position vs. upright tilt.

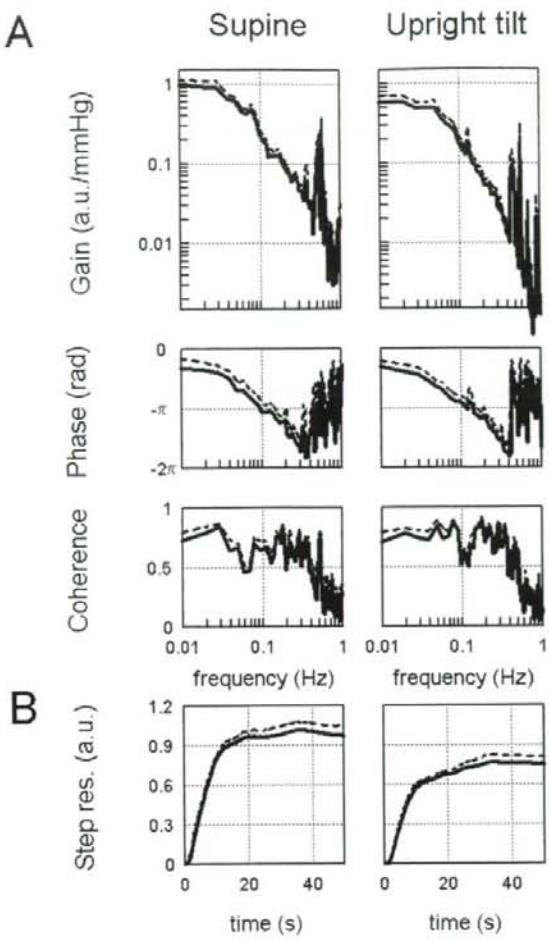

Fig. 4. A: The transfer function of the baroreflex peripheral arc from SNA to AP averaged from all animals (n = 8) in supine (left panels) and 60° upright tilt (right panels) positions. The gain plots (top), phase plots (middle), and coherence function (bottom) are shown. Upright tilt decreases the gain below the frequency of 0.1 Hz. **B**: Step responses (Step res.) derived from the transfer function corresponding to the transfer function shown in A. Upright tilt attenuates the response. Solid and dashed lines represent the mean and mean + SD values, respectively. a.u., arbitrary unit.

The baroreflex peripheral arc

Figure 4A shows the transfer function of the baroreflex peripheral arc from SNA to AP averaged from all animals. In both supine and upright tilt positions, the transfer gain decreased as the input frequency increased for the frequency range of 0.01 to 1 Hz, indicating low-pass characteristics. Upright tilt decreased the transfer gain between 0.01 and 0.1 Hz (Table 2). In both positions, the phase approached zero radian at the lowest frequency reflecting an increase in SNA with increased AP, and lagged as the input frequency increased. The coherence was over 0.5 for the frequency range of 0.01 to 1 Hz. Upright tilt did not affect the phase or coherence. Figure 4B shows the step response of AP corresponding to the transfer function shown in Fig. 4A. In both positions, the AP response increased gradually to reach a steady state. Upright tilt decreased the steady-state AP.

Table 2. Transfer function of baroreflex peripheral arc (from SNA to AP) in supine and upright tilt positions.

	Supine	Upright tilt
Gain (mmHg/au)		
0.01 Hz	0.97 ± 0.09	0.63 ± 0.06*
0.1 Hz	0.23 ± 0.03	0.15 ± 0.03*
0.3 Hz	0.04 ± 0.006	0.03 ± 0.003
Phase (rad)		
0.01 Hz	–0.79 ± 0.16	–0.69 ± 0.07
0.1 Hz	–2.83 ± 0.14	–2.58 ± 0.15
0.3 Hz	–4.74 ± 0.18	–4.63 ± 0.08
Coherence		
0.01 Hz	0.72 ± 0.07	0.71 ± 0.03
0.1 Hz	0.64 ± 0.08	0.62 ± 0.04
0.3 Hz	0.61 ± 0.08	0.68 ± 0.02
Step response (mmHg)		
Steady-state level	–0.97 ± 0.06	–0.75 ± 0.06*

Values are mean ± SD (n = 10). *P < 0.05; supine position vs. upright tilt.

The total baroreflex arc

Figure 5A shows the transfer function of the total baroreflex arc from CSP to AP averaged from all animals. In both supine and upright tilt positions, the transfer gain decreased as the input frequency increased for the frequency range from 0.01 to 1 Hz, indicating low-pass characteristics. Upright tilt did not affect the transfer gain (Table 3). In both positions, the phase approached –π radians at the lowest frequency reflecting negative feedback attained by the total baroreflex loop, and lagged as the input frequency increased. The coherence was over 0.5 for the frequency range from 0.01 to 0.2 Hz. Upright tilt did not affect the phase or coherence. Figure 5B shows the step response of AP corresponding to the transfer function shown in Fig. 5A. In both positions, the AP response increased gradually to reach a steady state. Upright tilt did not affect the step response.

The right column of Table 3 shows a simulation of the total arc transfer function in the absence of resetting in the neural arc. The simulation was based on the neural arc transfer function in supine position and the peripheral arc transfer function in upright tilt position. Without the resetting, the upright tilt would decrease the transfer function gain and would attenuate the step response of AP at steady state, compared with the values in supine position and those in upright tilt position with resetting.

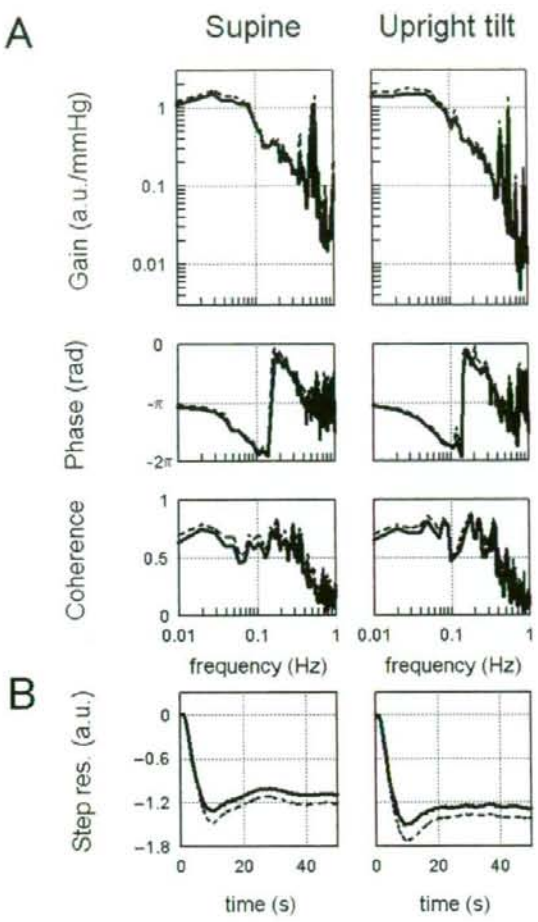

Fig. 5. A: The transfer function of the total baroreflex arc from CSP to AP averaged from all animals (n = 8) in supine (left panels) and 60° upright tilt (right panels) positions. The gain plots (top), phase plots (middle), and coherence function (bottom) are shown. **B**: Step responses (Step res.) derived from the transfer function corresponding to the transfer function shown in A. The transfer function and step response are similar in the supine and upright tilt positions. Solid and dashed lines represent the mean and mean + SD values in A and mean – SD values in B, respectively. a.u., arbitrary unit.

DISCUSSION

Arterial baroreflex is obviously a pivotal mechanism for maintaining AP under orthostatic stress against gravitational fluid shift and pressure disturbance [1, 2, 4], but the baroreflex function and its modulation in upright position are not fully understood. We previously reported that 60° upright tilt resets the steady-state characteristics of the baroreflex neural arc to a higher SNA [5]. However, the dynamic characteristics of the baroreflex system, which is a hallmark of fast-acting neural systems, in upright posture remain to be elucidated. Accordingly, in the present study, we identified the transfer function of the total baroreflex system and its two subsystems. The new major findings are that a 60° upright tilt increases the transfer gain of the baroreflex neural arc (CSP to SNA), decreases the transfer gain of the peripheral arc (SNA to AP), and as a result maintains the dynamic characteristics of the total baroreflex feedback system. These findings support our hypothesis that upright tilt resets dynamic transfer function of baroreflex neural arc to minify the pressure disturbance in total baroreflex control. These results were not affected by the order of postures, since returning the ani-

Table 3. Transfer function of total baroreflex arc (from CSP to AP) in supine, upright tilt and simulated upright tilt positions.

	Supine	Upright tilt	Simulated upright tilt without resetting of the neural arc
Gain (a.u./mmHg)			
0.01 Hz	1.10 ± 0.12	1.38 ± 0.18	0.71 ± 0.18*#
0.1 Hz	0.63 ± 0.09	0.69 ± 0.12	0.41 ± 0.13*#
0.3 Hz	0.15 ± 0.03	0.15 ± 0.03	0.11 ± 0.04*
Phase (rad)			
0.01 Hz	−3.33 ± 0.11	−3.29 ± 0.07	−3.21 ± 0.10
0.1 Hz	−5.76 ± 0.20	−5.55 ± 0.10	−5.51 ± 0.15
0.3 Hz	−1.98 ± 0.25	−1.87 ± 0.23	−1.91 ± 0.24
Coherence			
0.01 Hz	0.63 ± 0.06	0.65 ± 0.05	
0.1 Hz	0.60 ± 0.10	0.61 ± 0.06	
0.3 Hz	0.53 ± 0.07	0.55 ± 0.04	
Step response (mmHg)			
Steady-state level	−1.09 ± 0.11	−1.29 ± 0.12	−0.67 ± 0.11*#

Simulated transfer function in the absence of neural arc resetting is calculated from the neural arc transfer function in supine position and the peripheral arc transfer function in upright tilt position. Values are mean ± SD (n =10). *P < 0.05; supine vs. simulated upright tilt, #P < 0.05; upright tilt vs. simulated upright tilt.

mal posture from 60° upright tilt to horizontal supine position restored the transfer functions to the magnitudes observed in the initial supine position (data not shown).

Little is known about the arterial baroreflex feedback system under orthostatic stress. Although earlier studies investigated the gains of baroreflex control of SNA [12–14], vascular resistance [15] and R-R interval [16], these gains are parts of the total baroreflex system, and thus are insufficient to explain the dynamics of the total arc of the baroreflex feedback system. In addition, no study has examined the phase function of baroreflex in the subsystems and the total system. Moreover, while earlier studies addressed baroreflex in relation to AP regulation under orthostatic stress, most of them evaluated the baroreflex in supine, and not orthostatic posture [14]. In the present study, we identified the transfer functions of the two baroreflex subsystems (the neural and peripheral arcs) in upright posture independently using the baroreflex open-loop technique. Moreover, by connecting the subsystem transfer functions in series and closing them, we revealed the dynamic characteristics of the total baroreflex arc.

Our actual and simulation data indicated that resetting of the baroreflex neural arc in upright posture increases the transfer function gain of the total baroreflex arc. In our experiments, the 60° upright tilt reset and nearly doubled the transfer gain of the neural arc. Although the upright tilt decreased the transfer gain of the peripheral arc, resetting in the neural arc counteracted it and consequently preserved the dynamic transfer gain of the total baroreflex arc (1.4, Table 3). In a simulation of a situation where resetting in the neural arc is absent (Table 3), a 60° upright tilt would decrease the total arc transfer gain. These findings suggest that resetting of the neural arc (that is, baroreflex control of SNA) with dynamic characteristics plays an im-

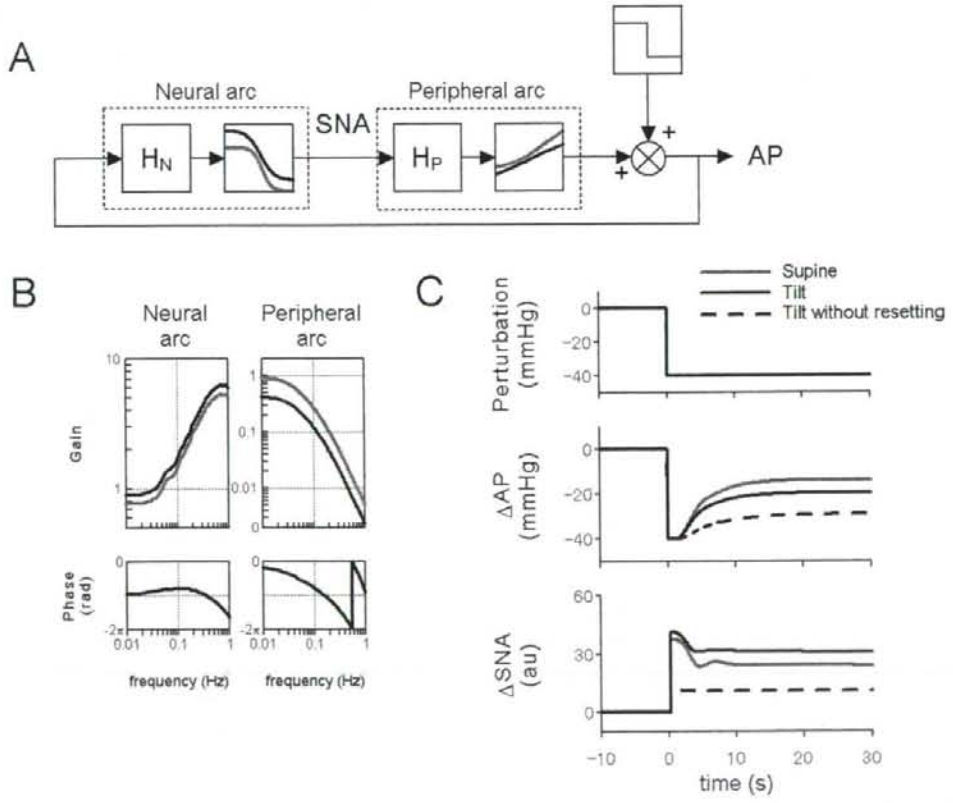

Fig. 6. A: Simulator of the baroreflex system during upright tilt. A stepwise perturbation was applied to the baroreflex negative feedback system (see APPENDIX for details). H_N, neural arc transfer function; H_P, peripheral arc transfer function. Nonlinear sigmoidal functions in the supine and upright tilt positions are shown by gray and black lines, respectively. **B**: Simulation results of integrated dynamic transfer function of linear-sigmoidal nonlinear cascade model in the neural (AP to SNA) and peripheral (SNA to AP) arcs in the supine (gray lines) and upright tilt (black lines) positions. **C**: Simulation results of a closed-loop AP and SNA responses to the stepwise pressure perturbation (–40 mmHg). The resetting during upright tilt (black line) would enhance SNA excitation as compared with the supine position (gray line) to minify a hypotension. Without the resetting in upright tilt, SNA responses would largely be attenuated to lead a hypotension.

portant role to maintain the dynamic transfer function of the total baroreflex system in upright posture.

A simulation of AP stability by baroreflex feedback control against pressure disturbance clearly suggests the importance of resetting of baroreflex neural arc in upright posture. Figure 6 shows the simulation of closed-loop baroreflex control of AP, when pressure disturbance was loaded to the peripheral cardiovascular compartment. According to an earlier study [17], we used the linear-sigmoidal nonlinear cascade model (Fig. 6A) to simulate the baroreflex dynamics. The result of simulation (Fig. 6B) was consistent with our in vivo findings that an upright tilt increased the dynamic transfer gain of the neural arc and decreased the dynamic gain of the peripheral arc. The simulation (Fig. 6C) shows that the baroreflex feedback system would minify the pressure disturbance (40 mmHg) by 50% or more in supine (14 mmHg) and upright tilt (19 mmHg) positions. However, without the resetting of the neural arc in upright tilt, the residual pressure disturbance (29 mmHg) would persist and the velocity of pressure response would become slower (Fig. 6C). These findings suggest that dynamic resetting of the neural arc increases the stability and quickness in response of orthostatic AP against pressure disturbance in closed-loop condition of the total baroreflex arc. In addition, the simulation indicates that the resetting would enhance increases in SNA in response to pressure disturbance in upright tilt compared to supine position (Fig. 6C). Without the resetting in upright tilt, the SNA response would be greatly attenuated (Fig. 6C). This suggests that resetting of the neural arc has a critical role in activating SNA appropriately to prevent hypotension by pressure disturbance during orthostatic stress.

Some explanations for the changes in baroreflex peripheral arc in upright tilt posture may be postulated. First, since the gravitational fluid shift toward the lower part of body (i.e., abdominal vascular bed, lower limbs) during upright posture decreases the preload and effective circulatory blood volume [1, 9], it may attenuate the dynamic transfer function from SNA to AP. Our actual data revealed that upright tilt decreased the transfer gain, but not the transfer phase, of the baroreflex peripheral arc (Fig. 4A). Therefore, upright tilt would blunt the magnitude of AP response to SNA without delaying the response, as shown in the calculated step response (Fig. 4B). Next, increases in humoral factors (i.e., catecholamine, angiotensin II) during upright posture could reduce the dependency of vascular resistance on neural control. However, intravenous infusion of angiotensin II did not affect the transfer function of baroreflex peripheral arc [18]. Moreover, intravenous infusion of catecholamine had no effects on the transfer function from sympathetic stimulation to heart rate [19]. These studies are consistent with the predominance of sympathetic neural control on cardiovascular pressor function [20].

Limitations

The present study has several limitations. First, we excluded the efferent effect of vagally mediated arterial and cardiopulmonary baroreflexes that may affect baroreflex control of SNA. Second, we used an anesthetic agent that may attenuate the baroreflex peripheral arc by reducing the cardiac pumping function, and may affect the neural arc gain. Third, since we sectioned the aortic depressor nerves to open the baroreflex feedback loop, the total baroreflex gain may be lower than the physiological level. Fourth, since we measured only renal SNA, our findings have limited applicability to other SNA. Although static [10, 21] and dynamic [21] regulation of the baroreflex neural arc is similar in renal, cardiac and muscle (vasoconstrictor) SNAs in supine posture, whether this holds true during orthostatic stress remains to be verified.

Lastly, we used rabbits that are quadrupeds. Since humans spend most of their time in nearly 90° upright postures whereas rabbits do not, our findings have limited applicability to humans. However, Japanese White rabbits spend most of their time in 10–40° head-up postures, and frequently stand up to nearly 70°. Since the denervation of both carotid and aortic arterial baroreflexes is known to cause severe postural hypotension at 60° upright tilt in quadrupeds [4], this suggests that even in quadrupeds, arterial baroreflex has a very important function in the maintenance of AP under orthostatic stress. Accordingly, despite the difference in species, our findings may reflect, at least, the qualitative aspects of orthostatic baroreflex physiology in humans. Indeed, recent human studies have suggested that orthostatic stress (lower body negative pressure) enhances the SNA response to AP change [22, 23] and increases baroreflex control of SNA (assessed by the relation between spontaneous changes in diastolic AP and SNA) [12] under baroreflex closed-loop condition.

In conclusion, the transfer function identified in baroreflex open-loop condition showed that 60° upright tilt increases the transfer gain of the baroreflex neural arc, decreases the transfer gain of the peripheral arc, and as a result maintains the dynamic characteristics of the total baroreflex feedback system. Simulation study suggests that resetting of the neural arc increases the transfer gain of the total baroreflex arc and also increases the stability of orthostatic AP against pressure disturbance. These findings suggest that upright tilt resets the dynamic transfer function of the baroreflex neural arc to maintain total baroreflex stability.

APPENDIX

To simulate the closed-loop AP response to stepwise pressure perturbation (Fig. 6), we used the linear-sigmoidal nonlinear cascade model [17].

We modeled the sigmoidal nonlinearity in the baroreflex neural arc by a four-parameter logistic function with

threshold according to our previous study [5] using the following equation:

$$y = \frac{P_1}{1+\exp[P_2(x-P_3)]} + P_4$$

where x and y are input (in mmHg) and output (in au) values. P_1 denotes the response range (in a.u.), P_2 is the coefficient of gain, P_3 is the midpoint of the input range (in mmHg), P_4 is the minimum output value of the symmetric sigmoid curve (in a.u.). We set $P_1 = 94$, $P_2 = 0.10$, $P_3 = 109$, $P_4 = 4$ in the supine position, and $P_1 = 112$, $P_2 = 0.09$, $P_3 = 109$, $P_4 = 29$ during upright tilt, according to our previous study [5].

The sigmoidal nonlinearity in the peripheral arc was modeled by a four-parameter logistic function using the following equation:

$$z = \frac{Q_1}{1+\exp[Q_2(y-Q_3)]} + Q_4$$

where y and z are input (in a.u.) and output (in mmHg) values. Q_1 denotes the response range (in mmHg), Q_2 is the coefficient of gain, Q_3 is the midpoint of the input range (in a.u.), and Q_4 is the minimum output value (in mmHg). We set $Q_1 = 115$, $Q_2 = -0.04$, $Q_3 = 63$, $Q_4 = 50$ in the supine position, and $Q_1 = 82$, $Q_2 = -0.05$, $Q_3 = 88$, $Q_4 = 50$ during upright tilt, according to our previous study [5].

In rabbits, the transfer function of the baroreflex neural arc (baroreceptor pressure to SNA) approximates derivative characteristics in the frequency range below 0.8 Hz, and high-cut characteristics of frequencies above 0.8 Hz [17]. Therefore, according to our previous study [17], we modeled the neural arc transfer function (H_N) using the following equation:

$$H_N(f) = -K_N \frac{1+\frac{f}{f_{c1}}j}{\left(1+\frac{f}{f_{c2}}\right)^2}\exp(-2\pi fjL)$$

where f and j represent the frequency (in Hz) and imaginary units, respectively; K_N is static gain (in a.u./mmHg); f_{c1} and f_{c2} ($fc_1 < f_{c2}$) are corner frequencies (in Hz) for derivative and high-cut characteristics, respectively; and L is a pure delay (in s) that would represent the sum of delays in the synaptic transmission through the baroreflex central pathways and the sympathetic ganglion. The dynamic gain increases in the frequency range of f_{c1} to f_{c2}, and decreases above f_{c2}. In simulations showed in Fig. 6, we matched K_N to the actual data in the supine and upright tilt positions in this study. We also set f_{c1}, f_{c2} and L at 0.05, 0.8 and 0.2, respectively, according to the present and previous studies [17].

In addition, the transfer function of the baroreflex peripheral arc (SNA to AP) approximates a second-order low-pass filter with the dead time as follows:

$$H_P(f) = K_P \frac{1}{1+2\zeta\frac{f}{f_N}j-\left(\frac{f}{f_N}\right)^2}\exp(-2\pi fjL)$$

where f_N and ζ are the neutral frequency (in Hz) and damping ratio, respectively; and L is a pure delay (in s). In simulations showed in Fig. 6, we matched K_P to the actual data in the supine and upright tilt positions in this study. We also set f_N, ζ and L at 0.07, 1.4 and 1.0, respectively, according to the present and previous studies [17].

The input amplitude of the stepwise pressure perturbation was –40 mmHg (Fig. 5, A and C, top panel). The closed-loop AP (Fig. 5C, middle panel) and SNA (Fig. 5C, bottom panel) responses were simulated up to 30 s.

This study was supported by the research project promoted by Ministry of Health, Labour and Welfare in Japan (#H18-nano-ippan-003), the Grants-in-Aid for Scientific Research promoted by Ministry of Education, Culture, Sports, Science and Technology in Japan (#18591992, #20390462) and the Industrial Technology Research Grant Program from New Energy and Industrial Technology Development Organization of Japan.

REFERENCES

1. Rowell LB. Human cardiovascular control. New York: Oxford Univ. Press, 1993.
2. Eckberg DL, Sleight P. Human baroreflexes in Health and Disease. New York: Oxford Univ. Press, 1992.
3. Persson P, Kirchheim H. Baroreceptor reflexes: integrative functions and clinical aspects. Berlin: Springer-Verlag, 1991.
4. Sato T, Kawada T, Sugimachi M, Sunagawa K. Bionic technology revitalizes native baroreflex function in rats with baroreflex failure. Circulation. 2002;106:730-4.
5. Kamiya A, Kawada T, Yamamoto K, Michikami D, Ariumi H, Uemura K, et al. Resetting of the arterial baroreflex increases orthostatic sympathetic activation and prevents postural hypotension in rabbits. J Physiol. 2005;566:237-46.
6. Sato T, Kawada T, Inagaki M, Shishido T, Takaki H, Sugimachi M, et al. New analytic framework for understanding sympathetic baroreflex control of arterial pressure. Am J Physiol. 1999;276:H2251-61.
7. Yamamoto K, Kawada T, Kamiya A, Takaki H, Miyamoto T, Sugimachi M, et al. Muscle mechanoreflex induces the pressor response by resetting the arterial baroreflex neural arc. Am J Physiol. 2004;286:H1382-8.
8. Ikeda Y, Kawada T, Sugimachi M, Kawaguchi O, Shishido T, Sato T, et al. Neural arc of baroreflex optimizes dynamic pressure regulation in achieving both stability and quickness. Am J Physiol. 1996;271:H882-90.
9. Sagawa K, Maughan L, Suga H, Sunagawa K. Cardiac contraction and the pressure-volume relationship. New York: Oxford Univ Press, 1988.
10. Kawada T, Shishido T, Inagaki M, Tatewaki T, Zheng C, Yanagiya Y, et al. Differential dynamic baroreflex regulation of cardiac and renal sympathetic nerve activities. Am J Physiol Heart Circ Physiol. 2001;280:H1581-90.
11. Glantz SA. Primer of Biostatistics (4th ed). New York: McGraw-Hill, 1997.
12. Ichinose M, Saito M, Fujii N, Kondo N, Nishiyasu T. Modulation of the control of muscle sympathetic nerve activity during severe orthostatic stress. J Physiol. 2006;576:947-58.
13. Fu Q, Shook RP, Okazaki K, Hastings JL, Shibata S, Conner CL, et al. Vasomotor sympathetic neural control is maintained during sustained upright posture in humans. J Physiol (Lond). 2006;577:679-87.
14. Mosqueda-Garcia R, Furlan R, Fernandez-Violante R, Desai T, Snell M, Jarai Z, et al. Sympathetic and baroreceptor reflex function in neurally mediated syncope evoked by tilt. J Clin Invest. 1997;99:2736-44.
15. Cooper VL, Hainsworth R. Carotid baroreceptor reflexes in humans during orthostatic stress. Exp Physiol. 2001;86:677-81.
16. Cooke WH, Hoag JB, Crossman AA, Kuusela TA, Tahvanainen KU, Eckberg DL.

Human responses to upright tilt: a window on central autonomic integration. J Physiol. 1999;517:617-28.
17. Kawada T, Yanagiya Y, Uemura K, Miyamoto T, Zheng C, Li M, et al. Input-size dependence of the baroreflex neural arc transfer characteristics. Am J Physiol Heart Circ Physiol. 2003;284:H404-15.
18. Kashihara K, Takahashi Y, Chatani K, Kawada T, Zheng C, Li M, et al. Intravenous angiotensin II does not affect dynamic baroreflex characteristics of the neural or peripheral arc. Jpn J Physiol. 2003;53:135-43.
19. Kawada T, Miyamoto T, Miyoshi Y, Yamaguchi S, Tanabe Y, Kamiya A, et al. Sympathetic neural regulation of heart rate is robust against high plasma catecholamines. J Physiol Sci. 2006;56:235-45.
20. Minson J, Chalmers J, Kapoor V, Cain M, Caon A. Relative importance of sympathetic nerves and of circulating adrenaline and vasopressin in mediating hypertension after lesions of the caudal ventrolateral medulla in the rat. J Hypertens. 1986;4:273-81.
21. Kamiya A, Kawada T, Yamamoto K, Michikami D, Ariumi H, Miyamoto T, et al. Muscle sympathetic nerve activity averaged over 1 minute parallels renal and cardiac sympathetic nerve activity in response to a forced baroreceptor pressure change. Circulation. 2005;112:384-6.
22. Ichinose M, Saito M, Ogawa T, Hayashi K, Kondo N, Nishiyasu T. Modulation of control of muscle sympathetic nerve activity during orthostatic stress in humans. Am J Physiol Heart Circ Physiol. 2004;287:H2147-53.
23. Ichinose M, Saito M, Kitano A, Hayashi K, Kondo N, Nishiyasu T. Modulation of arterial baroreflex dynamic response during mild orthostatic stress in humans. J Physiol. 2004;557:321-30.

Neuroscience Letters 439 (2008) 13–17

Contents lists available at ScienceDirect

Neuroscience Letters

journal homepage: www.elsevier.com/locate/neulet

Decoding rule from vasoconstrictor skin sympathetic nerve activity to nonglabrous skin blood flow in humans at normothermic rest

Atsunori Kamiya[a,b,*], Daisaku Michikami[a,b], Satoshi Iwase[b,c], Tadaaki Mano[b,d]

[a] Department of Cardiovascular Dynamics, National Cardiovascular Center Research Institute, Suita 565-8565, Japan
[b] Research Institute of Environmental Medicine, Nagoya University, Nagoya 464-8601, Japan
[c] Department of Physiology, Aichi Medical University, Aichi 480-1195, Japan
[d] Gifu University of Medical Science, Gifu 501-3892, Japan

Neuroscience Letters 439 (2008) 13–17

Contents lists available at ScienceDirect

Neuroscience Letters

journal homepage: www.elsevier.com/locate/neulet

Decoding rule from vasoconstrictor skin sympathetic nerve activity to nonglabrous skin blood flow in humans at normothermic rest

Atsunori Kamiya[a,b,*], Daisaku Michikami[a,b], Satoshi Iwase[b,c], Tadaaki Mano[b,d]

[a] Department of Cardiovascular Dynamics, National Cardiovascular Center Research Institute, Suita 565-8565, Japan
[b] Research Institute of Environmental Medicine, Nagoya University, Nagoya 464-8601, Japan
[c] Department of Physiology, Aichi Medical University, Aichi 480-1195, Japan
[d] Gifu University of Medical Science, Gifu 501-3892, Japan

ARTICLE INFO

Article history:
Received 13 February 2008
Received in revised form 4 April 2008
Accepted 6 April 2008

Keywords:
Cutaneous circulation
Skin blood flow
Skin sympathetic nerve activity
Transfer function
Vasoconstriction

ABSTRACT

Although an importance of vasoconstrictor skin sympathetic nerve activity (SNA) in control of cutaneous circulation is widely recognized, the decoding rule that translate dynamic fluctuations of vasoconstrictor skin SNA into skin blood flow is not fully understood. In 10 male subjects who rested in supine position under normothermic condition, we measured skin blood flow index (by laser-Doppler flowmetry) at the dorsum pedis, and vasoconstrictor skin SNA (by microneurography) that was confirmed to innervate the same region as the flow index. We determined the transfer and coherence functions from the neural activity input to the flow and quantified the contribution and predictability from the input to output by system engineering technique. The results showed that in frequency-domain analysis, the transfer function from vasoconstrictor skin SNA to skin blood flow had low-pass filter characteristics with 3.6 ± 0.1 s of pure time delay. The coherence function was approximately 0.5 between 0.01 and 0.1 Hz and less above 0.1 Hz. In time-domain analysis, the predictability from the SNA to the skin blood flow was approximately 50%. These findings indicate that at normothermic rest, the decoding rule from vasoconstrictor skin SNA to skin blood flow of skin is characterized by low-pass filter with 3–4 s of pure time delay, and that the vasoconstrictor skin SNA contributes to a half of fluctuation of skin blood flow in the condition. The incomplete dependence of skin blood flow on vasoconstrictor skin SNA may confirm nonneural mechanisms to control cutaneous circulation even at normothermic rest.

Human skin sympathetic nerve activity (SNA) has an important role in control of cutaneous circulation [6]. Although skin SNA contains several functional components, vasoconstrictor skin SNA is predominant during normothermic condition and cold stress [6,11,16], whereas sudomotor [6,11,16], and, in some case, vasodilator [14] skin SNA is predominant during heat stress. Although activation of vasoconstrictor skin SNA strongly decreases skin blood flow during cold stress [3], the vasoconstrictor activity also regulates the flow in normothermic condition [4]. However, the decoding rule that translate vasoconstrictor skin SNA into skin blood flow is not fully understood, probably because of ceaseless fluctuations of the nerve activity and the flow. The vascular response to nerve activity includes several time-dependent dynamic processes; release of neurotransmitter (noradrenaline) from presynaptic membrane, binding of neurotransmitter to specific adrenergic receptors in postsynaptic membrane, following cellular responses and resultant changes in microcirculation [12]. Accordingly, we hypothesized that the decoding rule (the transfer function from vasoconstrictor skin SNA to skin blood flow) at normothermic rest has low-pass filter characteristics with a few seconds of pure time delay.

In addition, although vasoconstrictor skin SNA is an important regulator of cutaneous circulation in normothermic condition, nonneural vascular reactions including vascular cutaneous autoregulation (e.g., venoarteriolar response [7,15], myogenic response [4]) also control cutaneous circulation. Although the vascular cutaneous autoregulation was mainly found during postural change [7,15] and forced respiratory maneuver [4], it is possible that these nonneural vascular mechanisms also controls cutaneous circulation even at supine rest. Accordingly, we hypothesized that the contribution of vasoconstrictor skin SNA to a fluctuation of skin blood flow at normothermic rest is limited to be moderate.

To test the two hypotheses, in resting supine posture under normothermic condition, we measured skin blood flow index (by laser-Doppler flowmetry) at the dorsum pedis, and vasoconstrictor skin SNA (by microneurography) that was confirmed to innervate the same region as the flow index. We determined the transfer and coherence functions from the neural activity input to the flow and

* Corresponding author. Tel.: +81 6 6833 5012; fax: +81 6 6835 5403.
E-mail address: kamiya@ri.ncvc.go.jp (A. Kamiya).

0304-3940/$ – see front matter © 2008 Elsevier Ireland Ltd. All rights reserved.
doi:10.1016/j.neulet.2008.04.018

quantified the contribution and predictability from the input to output by system engineering technique.

Subjects were 10 healthy male volunteers with age of 24 ± 4 (mean ± S.D.) year, height of 171 ± 6 cm, and weight of 65 ± 6 kg. We evaluated all subjects as healthy by completing a detailed medical history and by conducting a physical examination, resting electrocardiogram, blood chemistry analyses and psychological testing. None of the subjects smoked or had experience of recreational drugs. All subjects gave informed consent to participate in this study, which was approved by the Ethical Committee of the Research Institute of Environmental Medicine, Nagoya University. The experiments were performed at the Research Institute of Environmental Medicine, Nagoya University, whereas the data were analyzed at the National Cardiovascular Center Research Institute.

Left carpus arterial blood pressure (JENTOW TOM-101, Nippon Colin, Nippon Colin, Japan) was measured continuously. Electrocardiogram (chest lead II, for calculation of R–R interval) and thermistor respirogram were also recorded continuously.

Skin blood flow was measured at the dorsum pedis of the right leg by laser-Doppler flowmetry (ALF 21, Advance, Tokyo). Although the laser-Doppler flow method does not provide absolute flow value, it accurately and continuously reflects changes in skin blood flow [8] that is uninfluenced by muscle blood flow [13]. Sweat rate (mg min^{-1} cm^{-2}) were also measured at the nearly same point (1 cm apart from the point for skin blood flow) by the ventilated capsule method (Kenz-Perspiro 201, Suzuken, Nagoya). The capsule with the cross-sectional area of 0.76 cm^2 was fixed by coupe-face tape. The dry air was drained from the bottle with a temperature (27 °C) as the same as the experimental room. Since the area for measurement was so small, the skin blood flow outside of this capsule was not affected by this air drainage.

Skin SNA were measured from the peroneal nerves of the right leg by microneurography technique [11,16]. Briefly, a tungsten microelectrode (model 26-05-1, Federick Haer and Co., Bowdoinham, ME) was inserted percutaneously into the muscle or skin nerve fascicles of the peroneal nerve at the popliteal fossa without anesthesia. Nerve signals were fed into a preamplifier (Kohno Instruments, Nagoya) with two active band-pass filters set between 500 and 5000 Hz and were subsequently monitored with a loudspeaker. Skin SNA was identified according to the following discharge characteristics [2,11,16]: (1) broad-based neural activity unrelated to the cardiac cycle, (2) afferent activity induced by gentle skin touch, but not in response to tapping of calf muscles, and (3) enhancement during arousal stimuli. Moreover, the skin SNA was confirmed to innervate the dorsum pedis by a response of afferent activity to gentle skin touch of the region and by a reduction of skin blood flow immediately after large bursts of skin SNA. The SNA signals were full-wave rectified, fed through a resistance–capacitance low-pass filter at a time constant of 0.1 s, and then stored on a DAT recorder (PC216Ax, Sony Magnescale, Japan) at a sampling rate of 1000 Hz, together with other variables.

Experiments were performed on 10:00 a.m. We instructed the subjects to refrain from eating for 3 h before the experiments. Subjects were allowed to rest in the supine position in the quiet experimental room. The room temperature was set at 27 °C, a thermoneutral temperature. Microneurography and other measurements were prepared. After 30 min of rest, variables were measured for more than 30 min.

Skin SNA burst was identified and their areas calculated using a computer program custom-built by our laboratory. Since the SNA signal was dependent on electrode position, it was expressed as an arbitrary unit (au). An average burst amplitude during the first 3 min was given 100 au, and other SNA signals during the experimental protocol were normalized to this value. Skin blood flow was quantified by laser-Doppler flowmetry values. The averaged flow value during the first 3 min was given 100 au, and other flow

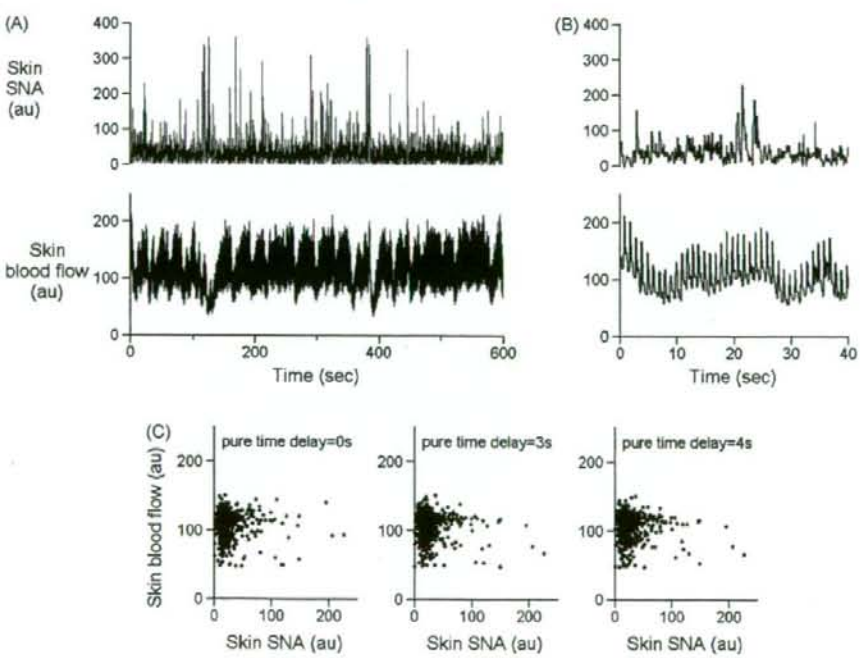

Fig. 1. (A) A typical example in one subjects of time series data of vasoconstrictor skin SNA and skin blood flow during 600 s of normothermic rest. au, arbitrary units. (B) Enlarged the data during the first 40 s of (A). (C) Scatter plotting of the skin SNA and skin blood flow (resampled at 1 Hz) of the same 600 s data as (A), with setting a pure time delay of 0 s (left), 3 s (middle) and 4 s (right).

values during the experimental protocol were normalized to this value.

Using the first 15 min of data, we calculated the transfer (the gain and phase) and coherence functions from skin SNA input to skin blood flow in frequency domain [9,10]. We resampled them at 10 Hz and segmented them into 10 sets of 50% overlapping bins of 2^{10} data point each. The segment length was 102.4 s, which yielded the lowest frequency bound of 0.01 (0.0097) Hz. We subtracted a linear trend and applied a Hanning window for each segment. We then performed fast Fourier transform to obtain frequency spectra of skin SNA and skin blood flow. We ensemble averaged the skin SNA power [Sxx(f)], skin blood flow power [Syy(f)], and cross power between them [Syx(f)] over 10 segments. Thereafter, we calculated the transfer function [$H(f)$] from skin SNA to skin blood flow as follows:

$$H(f) = \frac{\mathrm{Syx}(f)}{\mathrm{Sxx}(f)}$$

To quantify the linear dependence between skin SNA and skin blood flow in the frequency domain, we calculated the magnitude-squared coherence function [Coh(f)] as follows:

$$\mathrm{Coh}(f) = \frac{|\mathrm{Syx}(f)|^2}{\mathrm{Sxx}(f) \cdot \mathrm{Syy}(f)}$$

The coherence value ranges from zero to unity. Unity coherence indicates a perfect linear dependence between skin SNA and skin blood flow, whereas zero coherence indicates total independence of these two signals.

To quantify the transfer characteristics in time domain, the step response and predicted response of skin blood flow to changes in skin SNA was calculated by the discrete from convolution integral as follows:

$$Y(t) = \sum_{\tau=1}^{N} h(\tau) \cdot X(t-\tau)$$

where $h(\tau)$ is the impulse response obtained by inverse fast Fourier transform of the transfer function [$H(f)$], N is the total number of data elements, τ is the convolution parameter and t is time in increments of 0.1 s (or 10 Hz). The prediction was performed on the 8 min of data that was randomly selected from the remaining data that was not used for the calculation of transfer function. The predicted skin blood flow was compared with the measured flow while calculating the linear correlation coefficient (r) and the root mean square (RMS) between them when the correlation was judged statistically significant by $p < 0.05$ [5].

Fig. 1A shows a typical example (10 min) of skin SNA and skin blood flow at normothermic rest in one subject. Fig. 1B enlarged the first 40 s of data. Activations of skin SNA (i.e., 110–130 s in Fig. 1A, 20–25 s in Fig. 1B) were followed by a significant reduction of skin blood flow, whereas sweat rate was nearly 0 throughout the experiment, suggesting that the skin SNA was vasoconstrictor activity. However, scatter plotting of 1 Hz skin blood flow over skin SNA shown in Fig. 1A had no significant correlation regardless of pure time delay (Fig. 1C). Similar findings were observed in all subjects ($n = 10$). Skin blood flow had a clear pulse oscillation, whereas skin SNA did not. Mean blood pressure (means ± S.E., 85 ± 3 mmHg), heart rate (66 ± 3 beats/min) and respiratory rate (15 ± 1 breaths/min) were stable during the experimental period.

Fig. 2A shows the autospectra of skin SNA and skin blood flow obtained from all subjects. When the frequency increased from 0.01 to 0.9 Hz, the power of autospectra of skin SNA decreased to approximately 10% of the level at the lowest frequency, whereas that of skin blood flow to approximately 1%. Fig. 2B shows the transfer and coherence functions from skin SNA input to skin blood flow. The gain function decreased from 0.01 to 0.1 Hz and showed steeper decline from 0.1 to 0.3 Hz, indicating the low-pass filter characteristics. The phase function approached to $-\pi$ at the lowest frequency, indicating the negative response of skin blood flow to changes in skin SNA. This was consistent with that the skin SNA observed was vasoconstrictor activity. The coherence function was approximately 0.5 from 0.01 to 0.1 Hz and was below 0.4 above 0.1 Hz.

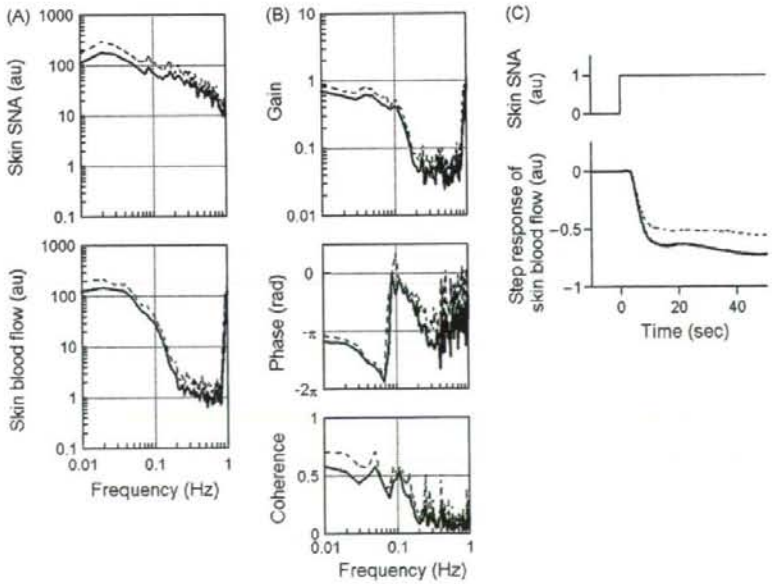

Fig. 2. (A) The autospectra of vasoconstrictor skin SNA and skin blood flow. (B) The gain, phase and coherence of transfer function from skin SNA to skin blood flow. (C) Step response of skin blood flow (to 1 au of step increase in skin SNA at time point 0). Values were shown as mean (solid line) + S.E. (broken line) in all panels ($n = 10$).

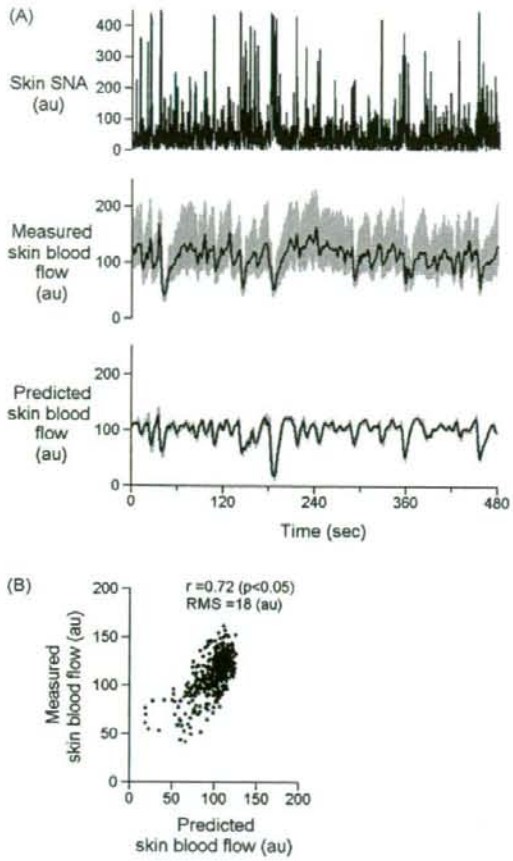

Fig. 3. (A) A typical example (8 min) of the measured vasoconstrictor skin SNA (top panel, 10 Hz) and skin blood flow (middle panel), and the predicted skin blood flow (bottom panel) from the calculated transfer function. The data shown was not used for the calculation of transfer function. In the panels of measured and predicted skin blood flow, gray and black lines show data resampled at 10 and 1 Hz, respectively. (B) Scatter plotting of the predicted and measured skin blood flow (resampled at 1 Hz) of the same data as (A).

Fig. 2C shows step response of skin blood flow (to 1 au of step increase in skin SNA at time 0). The step response had 3.6 ± 0.1 s of a pure time delay and decreased to reach -0.72 ± 0.16 au, that was consistent with the gain function at the lowest frequency. The decreasing response was consistent with the phase function in Fig. 2B.

To quantify the predictability of transfer function from skin SNA input to skin blood flow, skin blood flow responses to 8 min of measured skin SNA (Fig. 3A, top) was predicted (Fig. 3A, bottom). The measured data (skin SNA, skin blood flow) were not used for calculating the transfer function shown in Fig. 2B. The predicted skin blood flow (Fig. 3A, bottom, black line) was moderately similar to the measured skin blood flow (Fig. 3A, middle, black line) while the flows were resampled at 1 Hz. Scatter plotting of these predicted and measured skin blood flows showed significant correlation with r of 0.72 and RMS of 18 au (Fig. 3C). The significant correlations were observed in all subjects with r of 0.7 ± 0.1 and RMS of 18 ± 4 au.

Although an importance of vasoconstrictor skin SNA in control of cutaneous circulation is widely recognized [6,11,16], the decoding rule that translate dynamic fluctuations of vasoconstrictor skin SNA into skin blood flow is not fully understood. The major findings of the present study were that (1) the transfer function from vasoconstrictor skin SNA to skin blood flow in resting normothermic condition had low-pass filter characteristics with 3.6 s of pure time delay (Fig. 2B and C), (2) the coherence function from the SNA to the skin blood flow was approximately 0.5 between 0.01 and 0.1 Hz and less above 0.1 Hz (Fig. 2B) and (3) the predictability from the SNA to the skin blood flow was approximately 50% (Fig. 3). These findings support our two hypotheses that in nonglabrous skin, the decoding rule from vasoconstrictor skin SNA to skin blood flow at normothermic rest has low-pass filter characteristics with 3–4 s of pure time delay, and that the contribution of vasoconstrictor skin SNA to a fluctuation of skin blood flow is limited to be moderate.

The transfer function calculated in this study from vasoconstrictor skin SNA to skin blood flow indicates that the sympathetically mediated skin vascular response has history and frequency dependences. Given the vasoconstrictor function of the skin SNA, instantaneous vasoconstrictor skin SNA could negatively correlate with instantaneous skin blood flow even in normothermic condition. However, no correlation was found in the relation between the nerve activity and the flow (Fig. 1C, left panel). This was not simply because of an inappropriate pure time delay since neither 3 nor 4 s of pure time delay improved the correlation (Fig. 1C, middle and right panels). These time-domain data suggested that skin blood flow at a certain time point is affected by a significant duration of history of vasoconstrictor skin SNA before the time point. In other words, the translation from vasoconstrictor skin SNA to skin blood flow is history dependent, and vary depending on the frequency. This was confirmed by the frequency-domain analysis (Fig. 2B). As the frequency increased, the gain of transfer function, that means a ratio of magnitudes of changes in skin blood flow in response to those in the SNA at the frequency, decreased from 0.01 to 0.3 Hz, indicating the low-pass filter characteristics of the system. The phase of transfer function supported the goodness of the analysis, since it approached to $-\pi$ at the lowest frequency, indicating the negative responsiveness of skin blood flow to the vasoconstrictor skin SNA. Moreover, in time-domain analysis, step response of skin blood flow (in response to 1 au of step increase in the skin SNA) had 3.6 s of pure time delay, initial steep drop and following stable reduction, that was likely characteristics of low-pass filter with pure delay. Accordingly, these findings indicate that sympathetically mediated skin vasoconstrictor response depends on the history and the frequency of skin SNA.

Although the present data determined the decoding rule from vasoconstrictor skin SNA to skin blood flow at normothermic rest, the contribution of the SNA to the flow was limited to be mild to moderate. In frequency-domain analysis, the coherence function was approximately 0.5 between 0.01 and 0.5 Hz, indicating that the SNA determined a half of the variability of skin blood flow in the frequency range. This was consistent with the prediction of skin blood flow from measured skin vasoconstrictor SNA in time domain (Fig. 3). Although the data used for the calculation of transfer function was different from those for the prediction, the predicted skin blood flow (Fig. 3A, bottom panel, black line, 1 Hz resampling) was approximately similar to that measured (Fig. 3A, middle panel, black line, 1 Hz resampling). The prediction had moderate accuracy since it had r of 0.7 and RMS of 18% (Fig. 3B). Since vasoconstrictor skin SNA lacked significant pulse fluctuation (Fig. 1B), the prediction from the nerve activity could not cover the pulse fluctuation measured in skin blood flow (Fig. 3A, middle, gray line, 10 Hz resampling).

The incomplete dependence of skin blood flow on vasoconstrictor skin SNA may confirm that cutaneous microcirculation is

also controlled by nonneural mechanisms even in the supine posture at normothermic rest. In addition to sympathetically mediated vasoconstriction, nonneurally vascular reactions including vascular cutaneous autoregulation (e.g., venoarteriolar response [7,15], myogenic response [4]) is known to regulate skin blood flow. However, the vascular cutaneous autoregulation in normothermic condition has been investigated in postural [7,15] and respiratory vascular responses [4] that were accompanied by a large change in perfusion pressure to the skin. Since in the present study the subjects kept resting in the supine posture without postural or respiratory stress, our results suggest that both sympathetic and nonneural mechanisms control cutaneous circulation even at normothermic rest.

Limitations. First, since we investigated sympathetic cutaneous vasoconstriction at the dorsum pedis (nonglabrous skin), our data cannot simply be applicable to the sympathetic control of cutaneous microcirculation in glabrous skin, that has different (in some case, higher) sympathetic innervation and anastomoses from nonglabrous skin [1]. Second, since we studied only males subjects, it is unclear whether our conclusion holds true with females. Lastly, since the activation of skin SNA in this study was associated with the decrease in skin blood flow and neither increases in skin blood flow nor sweat rate, the SNA would include vasoconstrictor activity as its dominant component. However, we cannot exclude the possibility that the SNA contained some of other nerve types (i.e., vasodilator, sudomotor and pilomotor activity). The possibility can relate with the observed incomplete coherence between the SNA and skin blood flow.

In conclusion, at normothermic rest, the decoding rule from vasoconstrictor skin SNA to skin blood flow in nonglabrous skin has low-pass filter characteristics with 3–4 s of pure time delay. The vasoconstrictor skin SNA contributes to a half of fluctuation of skin blood flow in the condition.

Acknowledgments

This study was supported by the research project promoted by Ministry of Health, Labour and Welfare in Japan (#H18-nano-ippan-003), the Grants-in-Aid for Scientific Research promoted by Ministry of Education, Culture, Sports, Science and Technology in Japan (#18591992) and the Industrial Technology Research Grant Program from New Energy and Industrial Technology Development Organization of Japan.

References

[1] I.M. Braverman, Ultrastructure and organization of the cutaneous microvasculature in normal and pathologic states, J. Invest. Dermatol. 93 (1989) 2S–9S.
[2] C. Cogliati, R. Magatelli, N. Montano, K. Narkiewicz, V.K. Somers, Detection of low- and high-frequency rhythms in the variability of skin sympathetic nerve activity, Am. J. Physiol. Heart Circ. Physiol. 278 (2000) H1256–H1260.
[3] S. Durand, S.L. Davis, J. Cui, C.G. Crandall, Exogenous nitric oxide inhibits sympathetically mediated vasoconstriction in human skin, J. Physiol. 562 (2005) 629–634.
[4] S. Durand, R. Zhang, J. Cui, T.E. Wilson, C.G. Crandall, Evidence of a myogenic response in vasomotor control of forearm and palm cutaneous microcirculations, J. Appl. Physiol. 97 (2004) 535–539.
[5] S.A. Glantz, Primer of Biostatistics, 4th ed., McGraw-Hill, 1997.
[6] K.E. Hagbarth, R.G. Hallin, A. Hongell, H.E. Torebjork, B.G. Wallin, General characteristics of sympathetic activity in human skin nerves, Acta Physiol. Scand. 84 (1972) 164–176.
[7] H. Jepsen, P. Gaehtgens, Postural vascular response in human skin: passive and active reactions to alteration of transmural pressure, Am. J. Physiol. 265 (1993) H949–H958.
[8] J.M. Johnson, W.F. Taylor, A.P. Shepherd, M.K. Park, Laser-Doppler measurement of skin blood flow: comparison with plethysmography, J. Appl. Physiol. 56 (1984) 798–803.
[9] A. Kamiya, T. Kawada, K. Yamamoto, D. Michikami, H. Ariumi, T. Miyamoto, S. Shimizu, K. Uemura, T. Aiba, K. Sunagawa, M. Sugimachi, Dynamic and static baroreflex control of muscle sympathetic nerve activity (SNA) parallels that of renal and cardiac SNA during physiological change in pressure, Am. J. Physiol. Heart Circ. Physiol. 289 (2005) H2641–H2648.
[10] T. Kawada, T. Shishido, M. Inagaki, T. Tatewaki, C. Zheng, Y. Yanagiya, M. Sugimachi, K. Sunagawa, Differential dynamic baroreflex regulation of cardiac and renal sympathetic nerve activities, Am. J. Physiol. Heart Circ. Physiol. 280 (2001) H1581–H1590.
[11] T. Mano, Microneurography as a tool to investigate sympathetic nerve responses to environmental stress, Aviakosmicheskaia i Ekologicheskaia Meditsina 31 (1997) 8–14.
[12] L.B. Rowell, Human Cardiovascular Control, Oxford Univ. Press, 1993, pp. 3–161.
[13] J.L. Saumet, D.L. Kellogg Jr., W.F. Taylor, J.M. Johnson, Cutaneous laser-Doppler flowmetry: influence of underlying muscle blood flow, J. Appl. Physiol. 65 (1988) 478–481.
[14] J. Sugenoya, S. Iwase, T. Mano, Y. Sugiyama, T. Ogawa, T. Nishiyama, N. Nishimura, T. Kimura, Vasodilator component in sympathetic nerve activity destined for the skin of the dorsal foot of mildly heated humans, J. Physiol. 507 (Pt 2) (1998) 603–610.
[15] S.F. Vissing, N.H. Secher, R.G. Victor, Mechanisms of cutaneous vasoconstriction during upright posture, Acta Physiol. Scand. 159 (1997) 131–138.
[16] B.G. Wallin, J. Fagius, Peripheral sympathetic neural activity in conscious humans, Annu. Rev. Physiol. 50 (1988) 565–576.